




Preparation and properties of heat-treated esterified wood flour/polylactic acid composites for FDM 3D printing

Feng Chen^{1,*} , Xiaohui Ni¹, Yinan Liu¹, Xinghua Xia^{1,2}, and Xun Gao³

¹School of Art and Design, Taizhou University, Taizhou 318000, People's Republic of China

²Faculty of Creative Technology and Heritage, Universiti Malaysia Kelantan, 16300 Bachok, Malaysia

³College of Civil Engineering, Hunan University, Changsha 410082, China

Received: 21 April 2022

Accepted: 6 June 2022

Published online:

1 August 2022

© The Author(s), under exclusive licence to Springer Science+Business Media, LLC, part of Springer Nature 2022

ABSTRACT

Poly(lactic acid) (PLA) and wood composites as biodegradable materials have limited applications due to the poor dispersity of wood flour (WF) in PLA matrix and weak adhesion. Thus, this study aims to prepare PLA/WF composite materials by combining high-temperature moist air (220 °C), A-187 silane coupling agent, and acetic anhydride with PLA and employing heat treatment (HT) and esterification methods. The effects of different treatment methods on the crystallization, thermal and mechanical properties, and hydrophobicity of the WF/PLA composites are studied. The addition of heat-treated esterified WF decreases the cold crystallization temperature, thermal stability, and water resistance of the composites. Compared with the untreated WF/PLA composite, the heat-treated esterified WF/PLA composite has 40% increase in tensile strength and 13% increase in flexural strength. HT combined with other modification methods significantly reduce the crystallinity of the composites and improve the compatibility between WF and PLA, resulting in excellent performance enhancement of the heat-treated esterified WF composites compared with the untreated composites. Thus, addition of a small amount of HT esterified WF to WF/PLA composites in 3D printing filament extruder enhances its plasticization property and toughness at low cost, suggesting the future wide applications of the material in 3D printing.

Handling Editor: Stephen Eichhorn.

Address correspondence to E-mail: chenfeng1984@tzc.edu.cn

<https://doi.org/10.1007/s10853-022-07419-x>

Introduction

Poly(lactic acid) (PLA), a biodegradable aliphatic polyester well suited for the production of disposable materials [1, 2], is typically prepared from fermented plant starch, such as wheat starch, potato starch, sweet potato starch, cornstarch, and dextrin [3]. Additionally, PLA can be extruded into filaments by 3D consumable extruder products and is easy to print [4, 5], making it an ideal 3D printing material. However, PLA is brittle and has poor toughness [6]. Its elongation at break is less than 10%, which limits its application in high plastic deformation, and PLA is expensive, which increases the production cost of materials and limits its commercial application of PLA materials [7]. Due to the increasing demand for the aesthetic appearance of 3D printing products, 3D printing materials based on composites reinforced by metals, ceramics, food, organic or inorganic fillers, and even human cells have been developed. Currently, natural products, such as starch and wood flour (WF), are blended with PLA to improve the biodegradability and reduce the cost of its composites [8], which has attracted increasing attention.

Wood flour (WF) is mainly composed of cellulose, hemicellulose, and lignin. Cellulose is a natural homopolymer consisting of D-anhydroglucose ($C_6H_{10}O_5$) [9]. In the supramolecular structure of cellulose, the hydroxyl groups of the molecular chains are bonded by hydrogen bonds to form a crystalline region with high crystallinity, thus giving WF incredible rigidity [10]. Lignin has effective and economical adhesion properties, which can be used as rubber reinforcement, plastic matrix reinforcement, adhesive, and dispersant [11]. Due to the excellent performance of wood, 3D printing filaments are commercialized as WoodFill and Laywoo-D3, which consist of around 30% recycled WF and around 65% PLA [12]. However, WF with certain moisture content in the composite is heated and evaporated to cause an interface cavity layer during fusing filament process; thus, 3D printing filaments based on wood flour/PLA composites suffer low dimensional stability, poor mechanical properties, carbonization, and filament plugging [13]. In addition, WF is highly hydrophilic and undergoes agglomeration because of its surface abundance of hydroxyl groups ($-OH$) [14]; thus, PLA containing nonpolar ester groups has poor interfacial

compatibility with WF [15]. Hence, it is necessary to take the interfacial compatibility and dispersion of WF into account. Many researchers have conducted studies on enhancing the compatibility between PLA and WF.

Treatment of WF is a hot frontier research topic. The main reasons for WF modification are due to the poor plasticity, poor thermal stability, and strong hygroscopicity of WF. WF treatment methods include physical and chemical methods. Physical methods involve modification of the physical morphology of wood flour, which include stretching, calendaring, heat treatment (HT), corona, low-temperature plasma, radiation, and other discharge technologies. On the other hand, chemical methods involve the modification of the chemical structure of wood flour through molecular design for WF to exhibit special physical and chemical properties. Chemical methods mainly include esterification, oxidation, etherification, graft copolymerization, and cross-linking of WF to introduce functional groups other than hydroxyl groups to destroy the crystallinity of cellulose and reduce hydrogen bonds within or between molecules. Heat treatment is a common physical method of WF modification. Han et al. [16], Gao et al. [17], and Kerner et al. [18] conducted steam treatment on WF. It was found that steam treatment can open a large number of hydrogen bonds in WF, reduce intermolecular interaction, and increase the reaction activity between WF and other materials. However, there were still micropores and uneven particle distribution at the phase interface of WF composites. Chen et al. [19, 20] modified WF by combining a silane coupling agent with high-temperature hot air. The silane coupling agent was grafted in the form of a chemical bond on the surface of WF treated with high-temperature hot air. Results showed that surface hydrophobicity was improved, and the hydroxyl number on the surface sharply decreased. However, the hydrogen bond in the crystalline structure of cellulose was not destroyed, resulting in the thermal decomposition temperature of WF being far lower than its hot melting temperature. Thus, WF undergoes thermal decomposition before melting, affecting the thermoplastic properties of its composites.

The cellulose content in wood is about 50%. The existence of a large number of hydroxyl functional groups in wood can esterify wood with organic acids and anhydrides to reduce its surface polarity and improve its affinity with plastics. The main

esterification methods include acetic anhydride method, thioacetic acid method, vinyl ketone method, and chloroacetyl method. Among them, the acetic anhydride method is the most widely used method at present. Through replacement of the hydroxyl group of cellulose with the acetyl group of anhydride, some hydroxyl groups in the wood cell wall can be esterified [21, 22]. Some researchers found that using dimethyl amide, dimethyl sulfoxide, and dimethyl anisole as catalysts, wood can be esterified with maleic anhydride (MA) and phthalic anhydride (PA) at room temperature to obtain esterified wood containing suspended carboxyl groups. The modified wood has significant fluidity at 160 °C and 115 MPa and can be hot pressed into plastic sheets [23, 24]. The hydroxyl groups on the surface of the treated fiber were replaced by the anhydride groups, which was flatter and smoother than that of the untreated fiber, reducing the polarity of the natural fiber [25]. Jebrane and Sebe [26] used vinyl acetate and acetic anhydride as acetylation reagents to esterificate pine WF. Results showed that cellulose was easier to be esterified under acetic anhydride, and acetic anhydride may react with the aromatic ring of lignin to produce impurities. Lee et al. [27] used polycaprolactone (PCL), poly(butylene-succinate-cobutylencarbonate), PLA, and WF to produce PCL-graft-MA and PLA-graft-MA as compatibilizers and develop esterified WF/PLA composites. These studies showed that the double bond of MA could be inserted into the backbone of PCL and reacted with methyl and methine carbons of PLA by radical grafting. Due to esterification and hydrogen bonding with hydroxyl groups on the WF surface, PLA/WF composites with good compatibility were prepared. However, most of the reports on WF modification deal with esterification that requires a large number of organic solvents. This not only increases the reaction cost and difficulty of product posttreatment but also poses environmental concerns. Moreover, cellulose is more prone to degradation under acidic conditions if the test scheme or condition control is improper. Guo et al. [28] dissolved PA with *N*-methylimidazole (NMI). NMI acts as a hydrogen-bond-breaking agent when dispersed into lignocellulosic fibers and as a catalyst for esterification. Then, after washing esterified lignocellulosic fibers with acetone, the wood fiber/biodegradable polymer composites with good mechanical properties and thermal flow properties

were produced. However, the organic solvent was difficult to retrieve.

Under acidic conditions, the selection of appropriate nucleophilic compounds (carboxylic acid or anhydride) and appropriate reaction conditions can reduce the hydroxyl content of the esterified WF and provide better thermoplasticity. They can improve the brittleness of WF/PLA composites and may also interact with polylactic acid or produce hydrogen bond. In addition, it is reported that the agglomeration and hydroxyl groups of WF can be reduced under high-temperature hot air treatment. The use of esterification and HT complex modification for PLA/WF composite preparation for 3D printing has not yet been reported. In order to increase the compatibility between WF and PLA, we used WF heat-treated at high temperature, WF modified with silane coupling agent (SCA), WF esterified with glacial acetic acid/acetic anhydride (AAH), WF modified with SCA and heat-treated at high temperature, and WF esterified with AAH and heat-treated at high temperature. The composite materials were prepared by a 3D printing filaments extruder and 3D printer. Through the mechanical property, crystallinity, contact angle, and surface energy measurements, we aimed to determine the best method and mechanism for the synthesis of PLA/WF composites.

Materials and methods

Materials

Poplar wood was obtained in Inner Mongolia, China. The raw material was pulverized and screened to 100–200 mesh (150–75 µm), 200–300 mesh (75–48 µm), and smaller than 300 mesh (< 48 µm) using a biomass fiber roller mill (MF-600, Northeast Forestry University, Harbin, China). PLA with a melting flow index of 7.0 g/10 min at 240 °C was purchased from Kaixili Plastic Co., Ltd., Dongguan, China. The lubricant TPW604 and polyolefin elastomer (POE) (density 0.870 g/cm³, melt index 1.1 g/min, melting point 53 °C) flexibilizer were purchased from Struktol Company of America, LLC (Stow, OH, USA). Glacial acetic acid and acetic anhydride were of analytical grade and purchased from Sinopharm Chemical Reagent Co., Ltd., Shanghai, China. The SCA A-187 was obtained from Momentive Performance Materials Inc., New York, USA. The physical

properties of the chemical additives are shown in Tables 1 and 2. MgCl_2 , NaNO_2 , NaCl , Na_2SO_4 , and 4-Cyclohexyl-1-butanol (Vaseline) were received from Tianjin Benchmark Chemical Reagent Co., Ltd., Tianjin, China.

High-temperature hot air treatment

The moisture content of WF was 210% after immersing in water for 24 h. Then, the WF was added into an impulse-cyclone high-temperature hot air treatment equipment (MQG-50, Jiangsu Jianda Drying Engineering Co., Ltd., Changzhou, China) until the final moisture content reached 1–3%. The treatment temperature, air velocity, and feeding rate were 220 °C, 11 m/s, and 120 kg/h, respectively. The poplar WF dried in an electric oven at a temperature of $103 \text{ °C} \pm 2 \text{ °C}$ for 6 h was used as a reference sample for high-temperature treatment. All samples were sealed in a vacuum plastic sealing bag.

Silane coupling agent treatment

The A-187 SCA solution was prepared using distilled water as the solvent in an A-187/water molar ratio of 1:3. Then, untreated and high-temperature heat-treated WF samples were added into a high-speed mixer. The SCA was added by spraying. The weight ratio of the coupling agent and wood powder was 5:95, and the mixing time was 30 min until the coupling agent and WF were completely mixed. Then, the treated WF was dried at $103 \text{ °C} \pm 2 \text{ °C}$ for 12 h in a drying oven (DHG-9070A, Shanghai Yiheng Technology Co., Ltd., Shanghai, China).

Esterification treatment

Using distilled water as the solvent, 5% acetic anhydride solution was prepared. Into a three-port flask,

Table 2 Chemicals listing

Chemical name	Molecular formula
Glacial acetic acid	$\text{C}_2\text{H}_4\text{O}_2$
Acetic anhydride	$\text{C}_4\text{H}_6\text{O}_3$
3-Methacryloxypropyltrimethoxysilane	$\text{C}_{10}\text{H}_{20}\text{O}_5\text{Si}$
Magnesium chloride	MgCl_2
Sodium nitrite	NaNO_2 ,
Sodium chloride	NaCl
Sodium sulfate	Na_2SO_4
4-Cyclohexyl-1-butanol [Vaseline]	$\text{C}_6\text{H}_{11}(\text{CH}_2)_4\text{OH}$

60 g of WF and 300 g of glacial acetic acid were added, and the mixture was heated at 40 °C in a water bath for activation. After half an hour of reaction, 120 g of acetic anhydride solution was added, and the mixture was heated to 75 °C in the water bath and reacted for 5 h. Then, the esterified WF was poured into a Buchner funnel and rinsed with deionized water for five times. Finally, the esterified WF was put into the oven for drying to a moisture content of 1%–3% to increase the lubricity of wood flour in the wire drawing machine and reduce brittleness.

Preparation of WF/PLA composites for 3D printing

According to different formulations as shown in Table 3, modified WF/PLA composites for use as 3D printing materials were prepared in a high-speed plastic mixer (SHR-5A, Zhangjiagang Baixiong Klimens Machinery Co., Ltd., Zhangjiagang, China) for 15 min to produce uniform composites.

The process of preparing WF/PLA composites for use as 3D printing materials is shown in Fig. 1. The mixture was granulated at 150 °C in a single-screw

Table 1 Physical properties of chemical additives

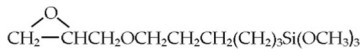
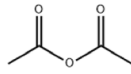
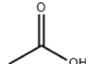
Chemical additives	Molecular structure formula	Molecular weight (g/mol)	Boiling point (°C)
Silane coupling agent (A-187)		32.12	290
Acetic anhydride		102.09	140
Glacial acetic acid		60.05	118

Table 3 Formulations for the preparation of modified wood flour/PLA composites for 3D printing materials

Sample	PLA (wt%)	HT WF (wt%)	SCA WF (wt%)	AAH WF (wt%)	HT-SCA WF (wt%)	HT-AAH WF (wt%)	POE (wt%)	TPW604 (wt%)
A	75	20					3	2
B	75		20				3	2
C	75			20			3	2
D	75				20		3	2
F	75					20	3	2

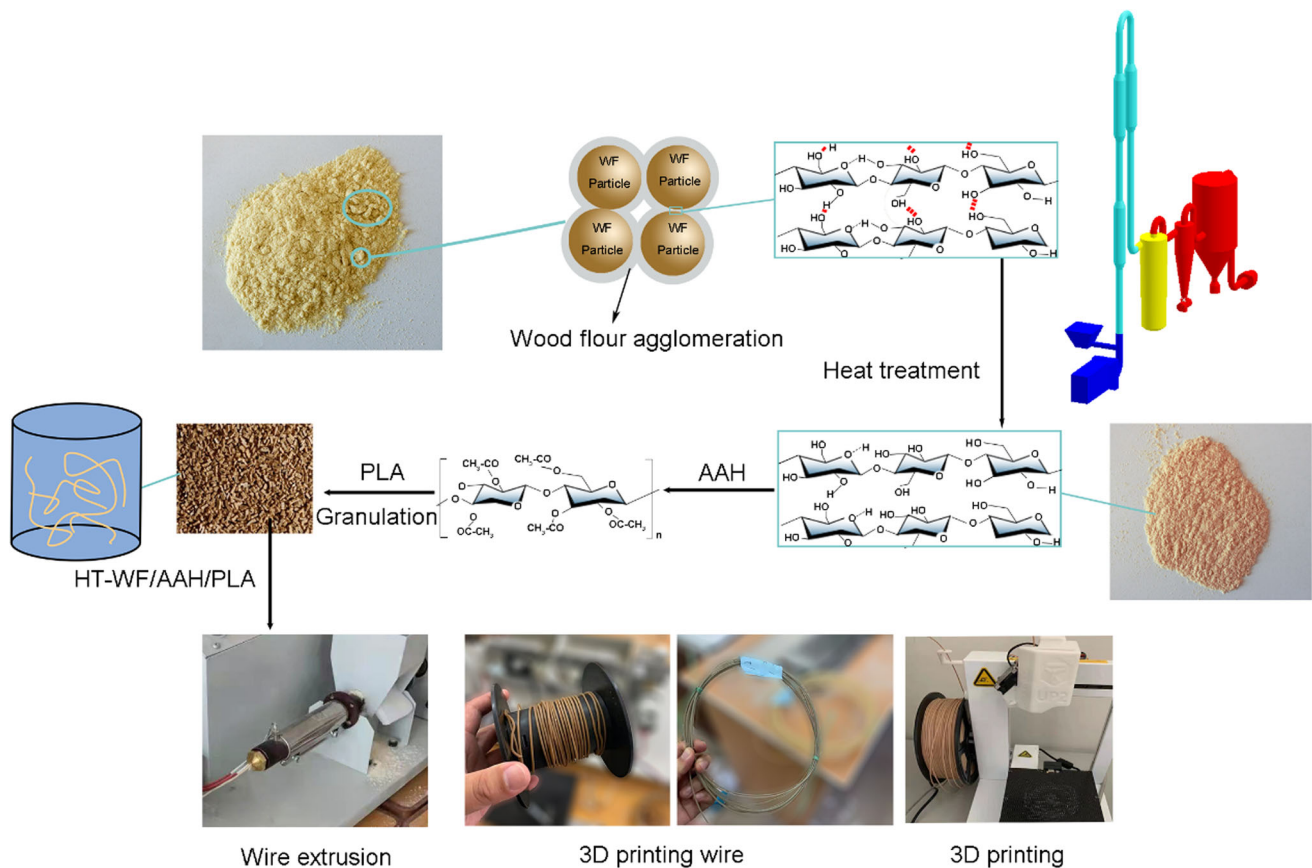


Figure 1 Process for the preparation of WF/PLA composites, involving wood powder agglomeration and weak interface layer damage.

extruder. The mixed particles were added into a single-screw 3D wire extruder (Suzhou Rongjie Technology Development Co., Ltd., Suzhou, China) to extrude the wire material through an aperture of 1.75 ± 0.02 mm. The temperature of zones 1–4 was set at 165 °C, 175 °C, 175 °C, and 170 °C, respectively, and the number of revolutions was 60. The extruded wire was then cooled using cooling water and placed in a box with constant temperature ($25 \text{ °C} \pm 2 \text{ °C}$) and humidity for 24 h.

SOLIDWORKS 2021 software (Dassault Systems, Shanghai, China) was used to draw a three-dimensional model of bending and stretching specimens, and the file was imported into the 3D printing control software ReplicatorG. The 3D printing direction, hot melt speed and temperature have certain effects on the mechanical properties. In order to reduce the effects of these parameters on the formula, we reinstalled the printing pad after removing the residual line material on the printing pad after each printing. Each time, the XYZ axis parameter of the printing

machine is reset to 0, and the printing direction is the length direction. The target temperature of the printing nozzle was set to 180 °C, and the layer height was set to 0.2 mm. The model was sliced into a Gcode code that can be recognized by the 3D printer 3DP-150 (Weinan Dingxin Creative Intelligent Manufacturing Technology Co., Ltd., Weinan, China). The WF/PLA composite wire was loaded into the wire feeding mechanism of the 3D printer. Finally, the entities of the bending and stretching specimens were printed out by stacking layers.

Mechanical strength testing

The mechanical strength of the 3D printing specimens was measured using a universal mechanical testing machine (WDM-20, Changchun Kexin Experimental Instrument Co., Ltd., Changchun, China). The tensile and flexural properties of the WF/PLA composites were measured according to GB/T1040-2006 and GB/T9341-2008, respectively.

Scanning electron microscopy

The morphologies of the specimen cross-sections were observed using a field-emission scanning electron microscope (ZEISS Sigma 300, Carl Zeiss AG, Oberkochen, Germany). After cooling the specimens with liquid nitrogen, all samples were coated with a thin layer of gold through sputtering before the scanning electron microscopy (SEM) imaging. An accelerating voltage of 30 kV was applied.

Fourier transform infrared spectroscopy

The modified WF and their composites with PLA were characterized by Fourier transform infrared (FT-IR) spectroscopy (Nicolet iN10, Thermo Scientific, Waltham, MA, USA) using finely ground samples (1%) in KBr pellets. A total of 32 scans in the range of 3500–400 cm^{-1} at a resolution of 4 cm^{-1} were collected for each sample.

Differential scanning calorimetry

The crystallization behavior and melting enthalpy of the WF/PLA composites were investigated using Diamond differential scanning calorimetry (DSC) (PerkinElmer Inc., Beaconsfield, UK) with the modulation option. The analysis was carried out under

nitrogen atmosphere. First, 3–5 mg of the specimen was weighed each time and was placed into the detector for testing. Then, the temperature was raised to 200 °C at a heatup rate of 10 °C/min and was maintained for 5 min to eliminate thermal history. Afterwards, the temperature was decreased to 25 °C at a rate of 10 °C/min and was maintained for 5 min. Finally, the temperature was again increased to 200 °C at a rate of 10 °C/min. The secondary temperature rise curve was then recorded, and crystallinity was calculated from the DSC curve using Eq. (1):

$$x_c = \frac{\Delta H_m}{w\Delta H_m^0} \times 100\% \quad (1)$$

where, ΔH_m is melting enthalpy, is the melting enthalpy of PLA at complete crystallization and the value is 93.6 J/g [29], and w is the mass fraction of polylactic acid in the sample.

Melt flow rate (MFR) testing

Melt flow rate is used to distinguish the fluidity of various thermoplastic materials in the molten state and can be used to characterize the plasticity of thermoplastic. According to GB 3682–2000, constant temperature of 15 min at 190 °C, 6 g of sample was loaded into the cartridge, after 4 min, the selected load was added on the piston after the temperature returned to the preset temperature. Samples were cut at 15 s/time, and the length of each cut section should be no shorter than 10 mm, preferably 10–20 mm. After cooling, the excised segments (at least 3) that remained were weighed one by one, to the nearest 1 mg, and their average mass was calculated as the melt MFR that was adopted in this experiment.

Contact angle testing

Contact angle was measured using a contact angle apparatus (Dataphysics Instrument Co., Ltd., Germany) with polyvinyl alcohol solution with a mass fraction of 7.5% as a volumetric solution. The samples modified by various types of silane were mounted on an aluminum sample holder, and a drop of polyvinyl alcohol solution was added to the surface. The contact angle of the specimen was measured after the specimen was properly balanced.

Results

FT-IR spectroscopy

Figure 2 shows the FT-IR spectra of the WF raw material, WF after one time of HT, WF after three times of HT, WF modified by HT-SCA, and WF modified by HT-AAH. It can be seen that the internal chemical structure of WF has changed greatly after HT. The absorption peak near 3432 cm^{-1} was attributed to the O–H stretching vibration. After HT for one time, the absorption intensity of the O–H peak of WF slightly decreased, indicating that one HA caused the “bridging reaction” of the hydroxyl groups between the cellulose microfibrils in the amorphous region of WF. However, after three heat treatments, the absorption intensity of the O–H peak increased. Lignin, cellulose, and hemicellulose were degraded to a certain extent, and the polysaccharide connecting bond in the crystalline region of cellulose broke, exposing more hydroxyl groups on the surface of WF. This provided the possibility for chemical reaction of hydroxyl groups. The degradation of cellulose and hemicellulose led to an increase in the absorption peak intensity at 1740 cm^{-1} , corresponding to the C=O vibration of carboxylic acid, hemicellulose, and polyxylose.

The characteristic peak at 1450 cm^{-1} was caused by the vibration of the benzene ring skeleton of lignin.

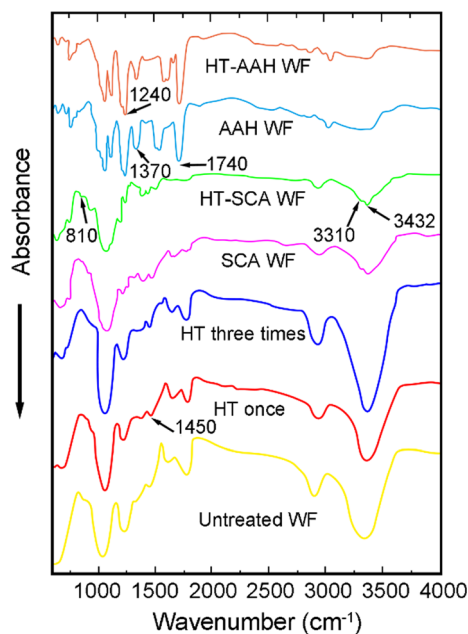


Figure 2 FT-IR spectra of WF with different treatments.

After HT treatment, the peak intensity increased, but it slightly decreased after three times of heat treatment. This indicated that the bond between lignin and hemicellulose broke to some extent, exposing part of lignin and increasing some benzene ring structural units in lignin. Furthermore, increasing the number of HT could lead to the degradation of lignin due to its continuous exposure to high-temperature and high-pressure hot air, and this results in a slight decrease in the absorption peak intensity caused by benzene ring skeleton vibration. Comparison of the results before and after A-187 SCA addition showed that the broad peaks at 3432 cm^{-1} of HT-SCA-modified WF, which were attributed to the active hydroxyl groups in WF, noticeably had reduced intensity. This indicated that a large amount of hydroxyl groups condensed with the silicon hydroxyl groups. In addition, a new characteristic absorption peak corresponding to the stretching vibration of Si–CH covalent bond appeared at 810 cm^{-1} , which proved the grafting reaction between WF and SCA. A large amount of hydroxyl groups on the surface of HT-AAH-modified WF were consumed, and the presence of C=O and $\text{CH}_3\text{--C=O}$ characteristic peaks at 1740 and 1370 cm^{-1} , respectively, proved the esterification reaction between WF and AAH.

Morphological characteristics of HT-AAH WF

It can be seen from Table 4 that the length, diameter, and aspect ratio of poplar WF significantly changed after esterification. After treatment with 5% acetic anhydride solution for 1.5 h, the length-to-diameter ratio of the heat-treated wood flour fiber was 4.66%, 8.34%, and 9.13% higher than that of HT WF with 100–200 mesh, 200–300 mesh, and more than 300 mesh, respectively. This is mainly due to the esterification process, where the acetyl group replaced some of the hydroxyl groups of wood flour, resulting in swelling effect that increases the volume of WF. At the same time, the acetic acid produced by the reaction accelerated the hydrolysis of cellulose. Because the strength of wood fiber has a significant correlation with the length and wall thickness of WF, the strength of WF increased with increasing thickness and length of cell wall, thus improving the comprehensive mechanical properties of the composites. The possible synthesis mechanism of HT-WF/AAH/PLA composite is shown in Fig. 3.

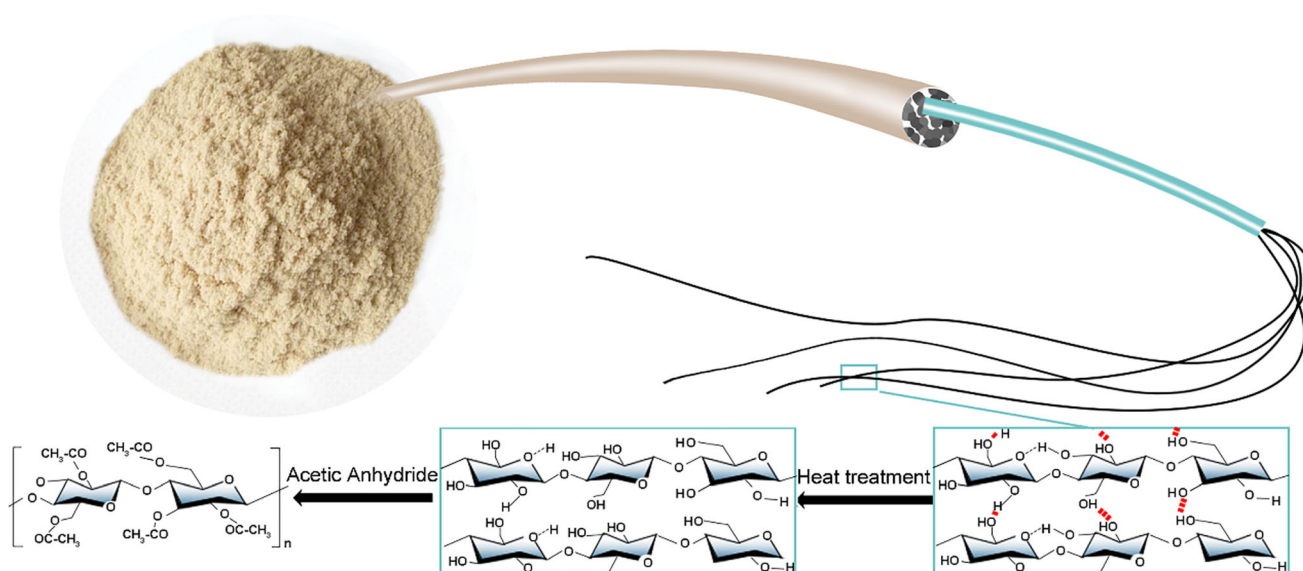
Table 4 Morphological characteristics of WF after Effects of HT-AAH modification

	Mesh	Morphological parameters	Maximum (mm)	Minimum (mm)	Average (mm)	RSD	CV(%)	Aspect ratio
HT-AAH WF	100–200	Length	0.463	0.412	0.446	0.021	4.71	3.304
		Diameter	0.146	0.127	0.135	0.010	7.38	
HT WF		Length	0.349	0.313	0.322	0.025	77.62	3.157
		Diameter	0.125	0.097	0.102	0.019	18.65	
HT-AAH WF	200–300	Length	0.302	0.241	0.275	0.028	10.21	3.313
		Diameter	0.088	0.075	0.083	0.006	7.23	
HT WF		Length	0.224	0.193	0.211	0.013	6.09	3.058
		Diameter	0.077	0.062	0.069	0.007	10.14	
HT-AAH WF	> 300	Length	0.219	0.187	0.198	0.014	7.16	3.250
		Diameter	0.064	0.054	0.061	0.003	4.96	
HT WF		Length	0.142	0.131	0.137	0.006	4.42	2.978
		Diameter	0.048	0.041	0.046	0.004	8.71	

SEM analysis

Figure 4 shows the SEM images with 400 times magnification of the tensile section of the modified products after injection molding under different treatment conditions. As can be seen from Fig. 4a, the surface of pure PLA was relatively flat and smooth, which was the characteristic of typical brittle materials. Figure 4b shows that the deformation of the matrix was not obvious, and HT WF was unevenly dispersed in the PLA matrix. It shows that the compatibility between esterified WF without HT and PLA was weak. Figure 4c, d shows the cross-sectional

micromorphology of WF/PLA after SCA and HT-SCA treatments. It can be seen that the cross-section of the composite treated with HT-SCA had obvious deformation, indicating that WF and PLA had good compatibility after heat treatment and addition of silane coupling agent. It can be seen from Fig. 4e that there were evenly distributed pores in the reaction section. It shows that esterification of WF by AAH improved the dispersion of WF in the plastic matrix. However, the surface of WF had almost no reactive groups, which resulted in weak interfacial adhesion and poor compatibility between WF and PLA. Figure 4f shows that the matrix section of HT-AAH-

**Figure 3** Possible synthesis mechanism of HT-AAH WF.

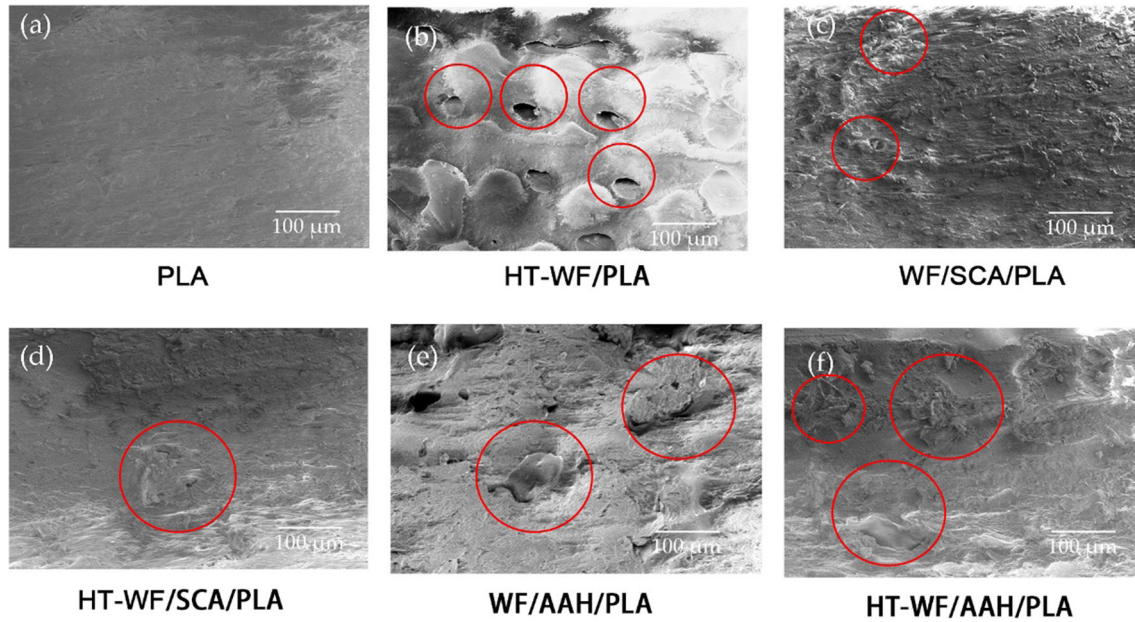


Figure 4 SEM images of the fracture surfaces of composites with different treatments.

modified WF/PLA composite presented more fibrous burrs, and the leaked particles were rough, which indicated that the stress of the composite could be fully transferred from PLA to wood flour and then absorbed by WF when it is subjected to external force. It shows that HT-AAH-modified WF had good compatibility with PLA.

DSC analysis

In order to study the thermal properties of the WF/PLA composites after different modification methods, the composites were characterized by DSC. The results are shown in Fig. 5. The two exothermic peaks at low temperature were the glass transition peak and the cold crystallization peak, where the temperature of the peak was the glass transition temperature (T_g) and cold crystallization temperature (T_{cc}), respectively. The endothermic peak at high temperature was the melting peak, and the peak temperature was the melting temperature (T_m).

The glass transition temperature (T_g) of the composites appeared at about 60 °C, which mostly occurred in the DSC curve of polyester polymers. Moreover, the cold crystallization temperature of the composites decreased with the addition of HT-SCA WF, indicating that the addition of HT-SCA WF enhanced the chain segment motion ability of the composites and made the composites crystallizable at

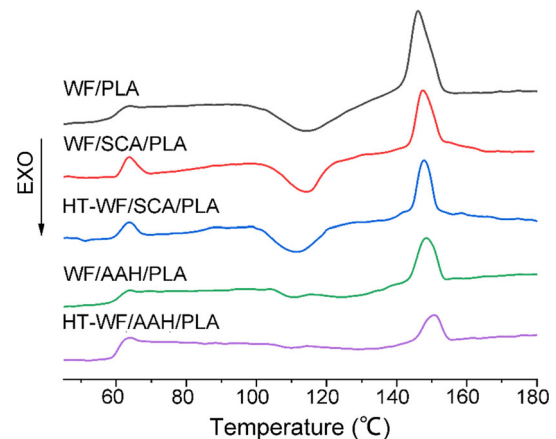


Figure 5 DSC curves of the WF/PLA composites after different treatments.

lower temperatures. The addition of SCA alone did not change the cold crystallization temperature of the composites, indicating that SCA had no effect on the nucleation and growth of the composites during crystallization.

It is known from the calculated results in Table 5 that the crystallinity x_c of composites all slightly decreased by different modification methods. It was indicated that these modification methods destroyed the crystalline structure inside the composites and effectively improved the interfacial compatibility between WF and PLA.

Appearance characteristics of composites

Figure 6 shows the appearance of pure PLA and modified WF/PLA composites. As shown in the figure, compared with the WF/PLA composite, the HT-WF/PLA composite was darker. Under the HT conditions, more color-generating groups such as hydroxyl, carbonyl, and carboxyl were produced. At the same time, the oxidation of lignin intensifies, which changed the wood powder color to dark. The color of the AAH-esterified WF/PLA composite was relatively light. For the SCA-modified WF/PLA composite, there was no great change in its color and appearance.

Mechanical performance

Figure 7 shows the tensile stress–strain curves of the composites. Figures 8 and 9 show the treatment methods of WF, which influence its tensile strength and flexural strength. From Fig. 7a, the mechanical property curves of PLA, WF/PLA composite, and HT-WF/PLA composite still exhibit the characteristics of brittle fracture and do not show stress yield. Compared with untreated WF/PLA composites, the heat-treated composites exhibited improved mechanical properties. The stress–strain curve of the heat-treated materials showed obvious yield inflection point and plastic deformation stress platform. From Fig. 7b, the tensile strength and elongation at break of HT-AAH/PLA composites increased with increasing WF meshes. These characteristics showed that the addition of esterified WF resulted in PLA change from a typical brittle material to a ductile material.

Melt flow analysis

Thermoplastic material is usually processed and molded in melt form, which requires the material to

be fluidized properly. In this experiment, the melt mass flow rate (MFR) of the composites was measured according to a polyethylene standard (temperature 190 °C, test load 21.6 kg). Due to the high molecular weight of PLA, chain entanglement or molecular chain interaction might occur in the molten state; thus, its MFR value in the molten state was higher.

Table 6 shows the melt MFR of different WF/PLA composites. At the treatment temperature of 190 °C, the untreated WF neither softened nor melted; thus, the untreated WF/PLA composites showed poor fluidity (0.1761). Compared with the MFR of pure PLA (4.3488), the MFR of the treated WF/PLA composites was lower. The main reason is that the surface of the treated WF was rough, and the friction was large when measuring the MFR. The esterified WF has thermoplasticity and compatibility with PLA resin. The fluidity of the esterified WF/PLA composite without HT (3.3293) was lower than that of the HT esterified wood flour/PLA composite (3.5878). This is because the distance between molecular chains in WF was small, and there were a lot of interaction forces such as hydrogen bonds. After esterification, the hydrogen bonds in the molecules of WF were broken, and acetic anhydride entered its crystal region to esterificate the hydroxyl group in the cellulose crystal region. In addition, due to the broken cellulose molecular chains of the heat-treated WF, the close arrangement of the original microfibrils was destroyed, and the inner cell wall layer showed an irregular noncrystalline structure. The more hydroxyl groups are available for esterification in the crystalline region, the more sufficient is the esterification reaction. In the molten state, the HT-AAH WF/PLA composites have obvious fluidity.

Figure 10a, b shows the relationship among viscosity, storage modulus, and frequency of treatments of the WF in the composites. The viscosity and modulus of the treated WF/PLA composites were lower than those of the untreated WF/PLA composites. After esterification, the hydroxyl groups on the surface of WF were replaced, and the plasticity of WF was improved. Thus, the composites had better fluidity at 190 °C, suggesting that their viscosity and modulus decrease. With the decrease in the number of hydroxyl groups, the hydrogen bond force between molecules in WF decreased. In this case, the strength of the network support of WF in the plastic

Table 5 Thermodynamic properties of the WF/PLA composites

Sample	T_g (°C)	T_{cc} (°C)	T_m (°C)	X_c (%)
WF/PLA	62.33	116.27	147.35	24.15
SCA WF/PLA	62.41	113.54	148.67	24.02
HT-SCA WF/PLA	62.26	112.18	148.81	23.61
AAH WF/PLA	62.74	110.98	149.70	23.83
HT-AAH WF/PLA	62.86	110.23	151.07	22.90



Figure 6 Appearance of the composites with different modifications.

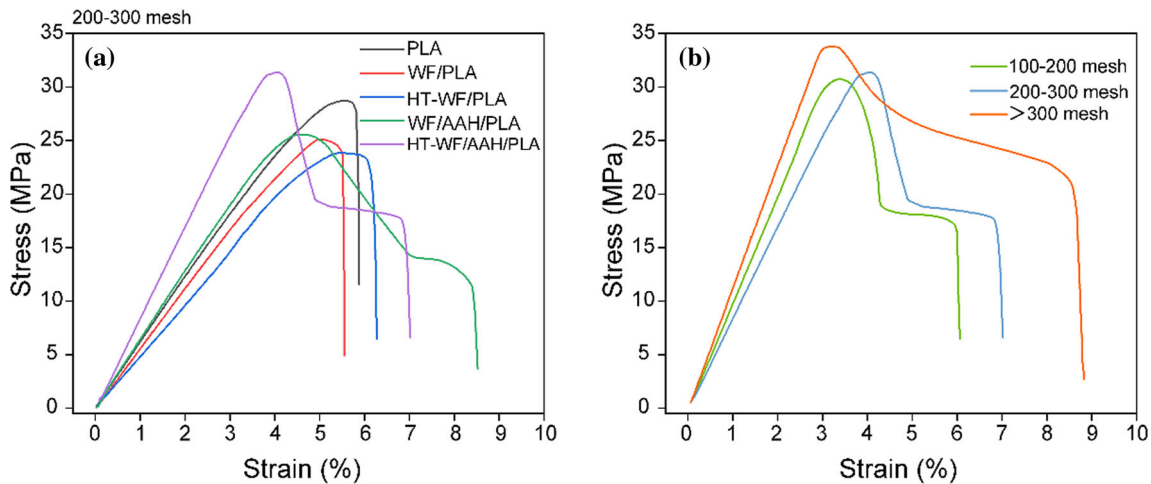


Figure 7 Tensile stress–strain curves of the **a** composites with different treatments and **b** HT-WF/AAH/PLA composites with WF of different mesh sizes.

matrix decreased, resulting in low modulus and viscosity.

Hydrophobicity analysis

Figure 11 shows the water contact angle of the treated WF/PLA composites. The contact angle of pure PLA was 82.1°. It can be seen that the hydrophobic properties of the untreated WF/PLA composites were poor. The minimum contact angle of the untreated WF/PLA composites was 69.3°, whereas that of the other three composites was improved, which was related to the reaction with the hydroxyl groups on the surface of SCA-treated and esterified WF.

Discussion

From the mechanical results in Figs. 8 and 9, when PLA and heat-treated SCA-modified WF and heat-treated esterified WF were combined, the tensile strength of HT-SCA/PLA and HT-AAH/PLA composites increased compared to that of SCA-modified WF and esterified WF that have not undergone HT. AAH and SCA can react with the heat-treated WF to form more covalent bonds. Although the interaction force and interface interaction between untreated WF and PLA were relatively poor, esterified WF could be fully dispersed in PLA matrix due to the improvement of its plasticity. These dispersed WF particles could absorb energy from the matrix, improving the

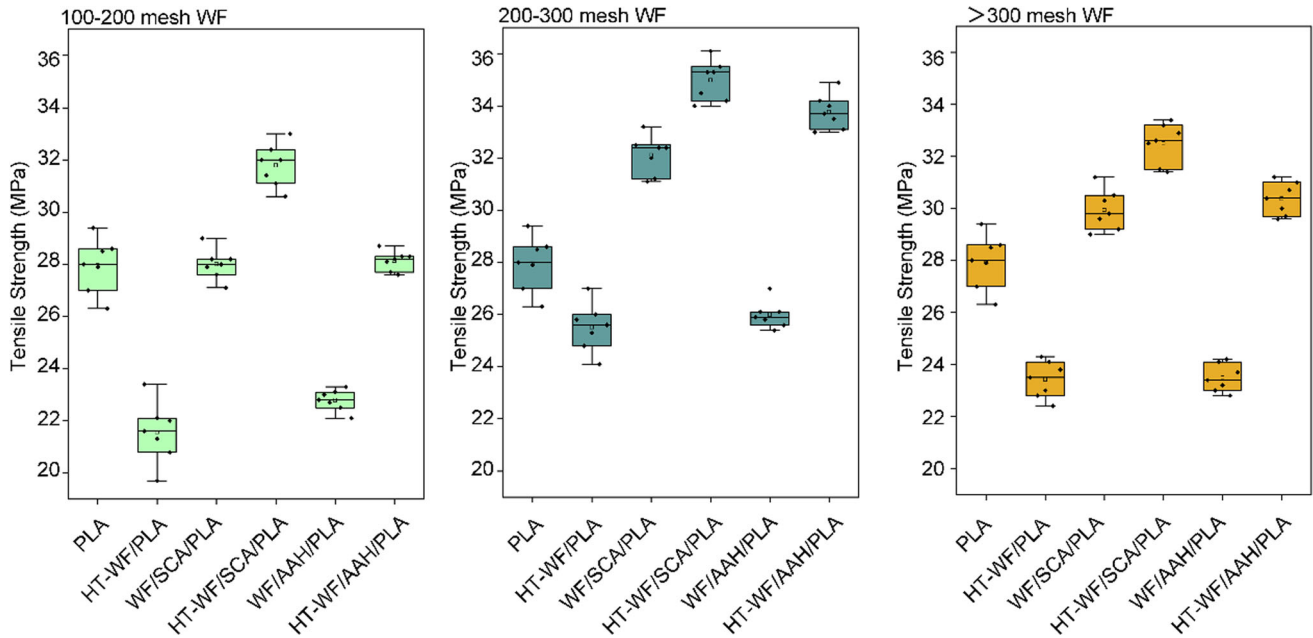


Figure 8 Treatment methods of WF influencing its tensile strength.

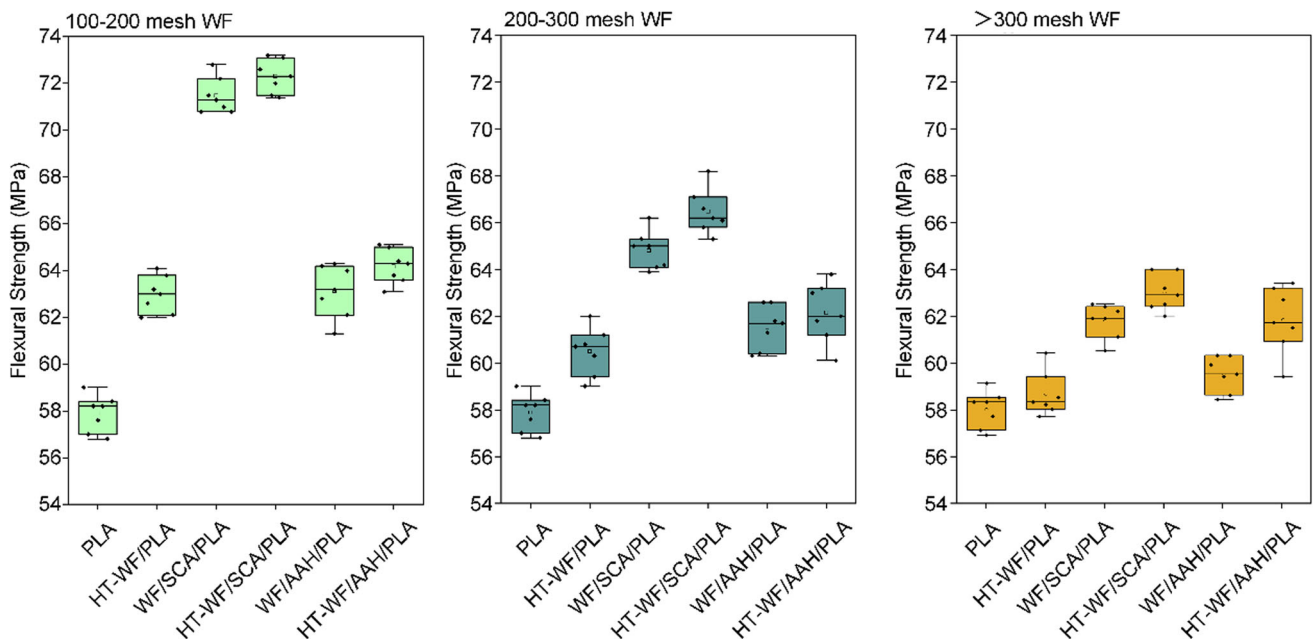


Figure 9 Treatment methods of WF influencing its flexural strength.

Table 6 Determination of melt mass flow rate of different WF/PLA composites

Sample	Temperature (°C)	Time interval (s)	Average weight (g)	MFR
WF/PLA	190	240	0.0705	0.1761
SCA WF/PLA	190	20	0.0639	1.9172
HT-SCA WF/PLA	190	20	0.0647	1.9423
AAH WF/PLA	190	10	0.0555	3.3293
HT-AAH WF/PLA	190	10	0.0598	3.5878
PLA	190	10	0.07248	4.3488

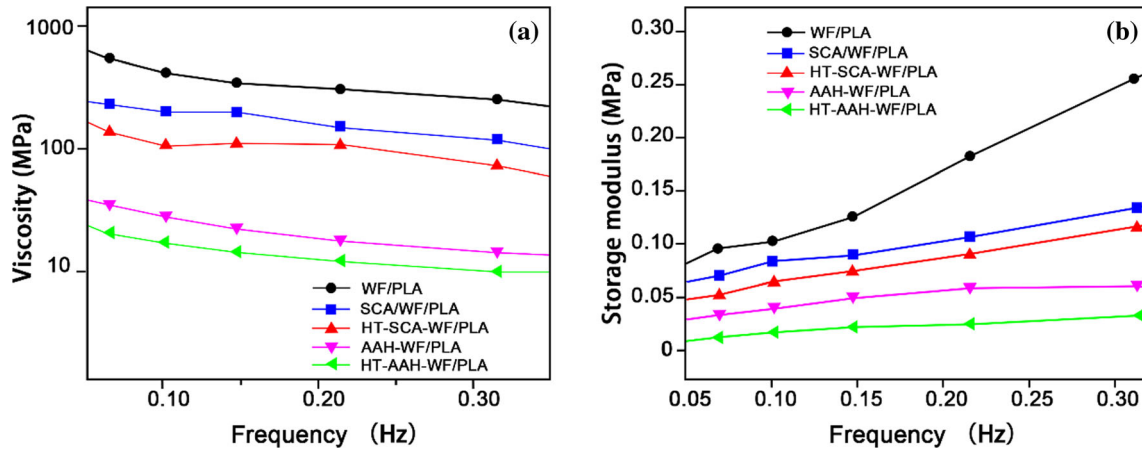


Figure 10 Effect of modified WF on the rheological properties of the composites. The relationship **a** between viscosity and frequency and **b** between storage modulus and frequency in the composites.

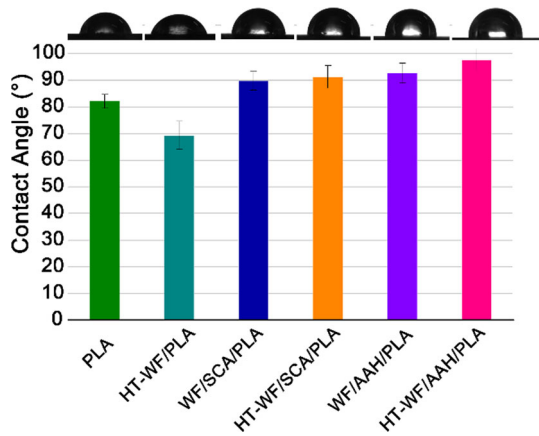


Figure 11 Contact angles of different WF/PLA composites.

tensile strength of the composites. In addition, the esterified WF increased the surface free energy of WF, which made it more closely in contact with PLA, and improved the compatibility of the two phases.

The flexural strength of the composites modified with SCA was significantly improved. However, the flexural strength of the composites from esterified WF was not significantly improved. The strength of the esterified WF/PLA composite was weaker than that of WF with less than 300 mesh size. For WF having 100 to 200 mesh size, the crystallization area was not fully opened. Thus, the plasticization degree of WF was incomplete, and its rigid material function was retained. However, with the increase in WF mesh size, the role of WF in bending performance became less significant, resulting in the decline of flexural strength. The flexural strength of modified WF after HT was higher than that of WF without HT.

After HT of WF, impurities such as pectin on the surface of WF could be removed by friction and thermal decomposition, which made the WF particles significantly smaller and increased surface roughness compared with the untreated WF. This produced more mechanical interlocks with PLA segments and further enhanced the PLA matrix.

The results of water contact angle in Fig. 11 showed that the hydrophobic properties of the HT-AAH WF/PLA composite were superior, and its contact angle was 97.5°. This was mainly related to the content of the hydroxyl groups in WF. The hydroxyl groups in the esterified WF were transformed into ester groups through acetylation reaction, which reduced the hydrogen bond between molecules in cellulose and reduced the hydrophilicity of the material. The esterified WF after HT had a large water contact angle. Under this condition, WF could be interspersed with PLA, and the space between molecular chains decreased, which hindered the entry of small molecules.

From DSC analysis in Fig. 5, when AAH-esterified WF was added to PLA, the strength of the cold crystallization peak significantly decreased, and the width of the cold crystallization peak widened. On the other hand, the introduction of ester groups on the cellulose molecular chain within AAH WF made AAH WF more flexible than WF. The rigid segments of AAH WF and the flexible segments of PLA were more fully intertwined with each other, and the overall flexibility of the molecular chain in the blended material was higher, thereby reducing the degree of cold crystallization. After high-temperature

treatment, the cold crystallization degree of the esterified WF was further reduced. This is because the WF cell wall could be displaced, deformed, and fibrillated under the HT conditions; thus, the microfibril-like structure disappeared more and the crystalline structure was destroyed.

From FT-IR analysis, due to the expansion of WF after esterification, the length-to-diameter ratio increased. During the thermal mixing process, PLA penetrated into the surface and internal voids of the expanded WF. Due to the reduced number of hydroxyl groups in HT-AAH-modified WF, WF became highly compatible with and highly dispersed in biomass polymers. HT and esterification can also assist in efficient thermoplastic processing of wood flour and effectively prevent loss of enhancement effect caused by damaged WF fiber structures during thermoplastic treatment of its composites. The possible synthesis mechanism of HT-WF/AAH/PLA composite is shown in Fig. 3. The main chemical components of poplar fiber are cellulose, hemicellulose, and lignin, which all have a large amount of hydroxyl groups and can be esterified with acetic anhydride. HT of WF destroys the hydrogen bond between molecules and within molecules and exposes more hydroxyl groups in WF. After HT and anhydride esterification, wood powder exhibits good thermoplastic properties and can be formed into filaments during wire extrusion. This shows that the biomass composites used to form wire rods for 3D printing can be successfully dispersed in PLA matrix using the modification methods presented in this study.

Conclusion

In order to further improve the compatibility of WF and PLA, the compatibilizers SCA and glacial acid/AAH were added to wood fiber after HT. The compatibilization mechanism of SCA and AAH was determined by infrared spectroscopy, and their effects on the mechanical, thermal, and mechanical properties of the WF/PLA composites were investigated. The effects of the WF modification treatments on the crystallization and water resistance of the WF/PLA were studied, and their section morphologies were characterized. The results are summarized below.

The infrared spectra show that the intensity of the absorption peak near 3432 cm^{-1} attributed to the O–H stretching vibration increases with increasing number of HTs. This indicates that heat treatment can expose more hydroxyl groups on the surface of WF, which provides the possibility for the chemical reaction of hydroxyl groups. The characteristic peaks at 1740 and 1370 cm^{-1} of WF treated with AAH proved the WF esterification with AAH.

By observing the change of aspect ratio, it can be seen that the acetyl groups replaced some of the hydroxyl groups in WF after esterification, resulting in swelling effect and increase in aspect ratio.

Several modification methods can improve the mechanical properties of the WF/PLA composites to varying degrees. The mechanical properties of the WF/PLA composites can be improved by HT, SCA treatment, and esterification of wood fiber. However, the effect of esterification on the WF/PLA composites is not obvious.

SEM images of the tensile section of the composites show that AAH-modified WF without HT improves the dispersion of WF in the plastic matrix. However, the compatibility of WF with PLA is limited, and the tensile section still shows poor compatibility between the two components. On the other hand, the compatibility between the esterified wood fiber and PLA after HT is good as shown by the rough tensile section and obvious matrix deformation in the SEM images. The appearance of a large number of cavities and relatively flat sections shows that the HT WF/PLA composites are still brittle materials, and their compatibility is poor.

The modification method did not change the crystal form of the modified WF/PLA composites. The crystallinity of the wood fiber was reduced after four treatments, and the crystallinity and cold crystallization temperature of the heat-treated and esterified wood fiber composites were the lowest. This is due to the enhanced movement of chain segments, the enhanced ability of penetration between phases, increased interaction force between components, and reduced surface adhesion of each interface in the composites in the heat-treated and esterified WF composites, resulting in greater compatibility between WF and PLA in HF-AAH/PLA.

The PLA and HT esterified WF composites exhibited the largest contact angle (97.5°) and superior hydrophobic properties.

Acknowledgements

The authors gratefully acknowledge financial supports from the National Natural Science Foundation of China (NSFC) (No.31901243) and Zhejiang Province Construction Project (No. 2020K163). Feng Chen conceived and designed the experiments; Yinan Liu and Xinghua Xia performed the experiments; Xiaohui Ni and Xun Gao analyzed the data and wrote the paper. We thank Editage (www.editage.com) for editing manuscript to ensure language and grammar accuracy.

References

- [1] Xu H, Shen M, Shang H, Xu W, Hakkarainen M (2021) Osteoconductive and antibacterial poly(lactic acid) fibrous membranes impregnated with biobased nanocarbons for biodegradable bone regenerative scaffolds. *Ind Eng Chem Res* 60(32):12021–12031. <https://doi.org/10.1021/acs.iecr.1c02165>
- [2] Gao S, Song W, Guo M (2020) The integral role of bio-products in the growing bioeconomy. *Ind Biotechnol* 16(1):13–25. <https://doi.org/10.1089/ind.2019.0033>
- [3] Rodrigues SCS, de Mesquita FAS, de Carvalho LH, Alves TS, Folkersma R, dos Araújo RS, Oliveira AD, Barbosa R (2021) Preparation and characterization of polymeric films based on PLA, PBAT and corn starch and babassu mesocarp starch by flat extrusion. *Mater Res Exp* 8(3):1–10. <https://doi.org/10.1088/2053-1591/abeaca>
- [4] Viidik L, Vesala J, Laitinen R, Korhonen O, Ervasti T (2020) Preparation and characterization of hot-melt extruded polycaprolactone-based filaments intended for 3D-printing of tablets. *Eur J Pharm Sci* 158:1–27. <https://doi.org/10.1016/j.ejps.2020.105619>
- [5] Kananathan J, Samykano M, Kadirgama K, Ramasamy D, Rahman MM (2022) Comprehensive investigation and prediction model for mechanical properties of coconut wood-poly(lactic acid) composites filaments for FDM 3D printing. *Eur J Wood Wood Prod* 80(1):75–100. <https://doi.org/10.1007/s00107-021-01768-1>
- [6] Natesan S, Samuel JS, Srinivasan AK (2021) Design and development of Schiff's base (SB)-modified poly(lactic acid) (PLA) antimicrobial film for packaging applications. *Polym Bull* 10:1–20. <https://doi.org/10.1007/s00289-021-03703-z>
- [7] Grijpma DW, Nijenhuis AJ, Wijk P, Pennings AJ (1992) High impact strength as-polymerized PLLA. *Polym Bull* 29(5):571–578. <https://doi.org/10.1007/BF00296720>
- [8] Lv S, Zhang Y, Gu J, Tan H (2017) Biodegradation behavior and modelling of soil burial effect on degradation rate of PLA blended with starch and wood flour. *Colloids Surf B Biointerfaces* 159:800–808. <https://doi.org/10.1016/j.colsurfb.2017.08.056>
- [9] Nh A, Ia B, Mg C, Gg D (2019) The remarkable three-dimensional network structure of bacterial cellulose for tissue engineering applications. *Int J Pharm* 566:631–640. <https://doi.org/10.1016/j.ijpharm.2019.06.017>
- [10] Xing L, Hu C, Zhang W, Guan L, Gu J (2019) Transition of cellulose supramolecular structure during concentrated acid treatment and its implication for cellulose nanocrystal yield. *Carbohydr Polym* 229:1–30. <https://doi.org/10.1016/j.carbpol.2019.115539>
- [11] Kumar AN, Kim GB, Muhorakeye A, Varjani S, Kim SH (2021) Biopolymer production using volatile fatty acids as resource: effect of feast-famine strategy and lignin reinforcement. *Biores Technol* 326(1):124736. <https://doi.org/10.1016/j.biortech.2021.124736>
- [12] Lam K (2015) MO-F-CAMPUS-I-03: CT and MR characteristics of some specialty 3D printing filaments. *Med Phys* 42(6):3579–3579. <https://doi.org/10.1118/1.4925469>
- [13] Tao Y, Wang H, Li Z, Li P, Shi SQ (2017) Development and application of wood flour-filled poly(lactic acid) composite filament for 3D printing. *Materials* 10(4):1–6. <https://doi.org/10.3390/ma10040339>
- [14] Elrhayam Y, Elharfi A (2019) 3D-QSAR studies of the chemical modification of hydroxyl groups of biomass (cellulose, hemicelluloses and lignin) using quantum chemical descriptor. *Heliyon* 5(8):1–7. <https://doi.org/10.1016/j.heliyon.2019.e02173>
- [15] Liu R, Luo S, Cao J, Chen Y (2016) Mechanical properties of wood flour/poly(lactic acid) composites coupled with waterborne silane-polyacrylate copolymer emulsion. *Holzforchung* 70(5):439–447. <https://doi.org/10.1515/hf-2015-0064>
- [16] Han G, Zhang C, Zhang D, Umemura K, Kawai S (1998) Upgrading of urea formaldehyde-bonded reed and wheat straw particleboards using silane coupling agents. *J Wood Sci* 44(4):282–286. <https://doi.org/10.1007/BF00581308>
- [17] Gao X, Li Q, Cheng W, Han G, Xuan L (2017) High temperature and pressurized steaming/silane coupling co-modification for wood fibers and its effect on the properties of wood fiber/HDPE composites. *Macromol Res* 25(2):141–150. <https://doi.org/10.1007/s13233-017-5024-x>
- [18] Xiang E, Huang R, Yang S (2021) Change in micromechanical behavior of surface densified wood cell walls in response to superheated steam treatment. *Forests* 12(6):1–13. <https://doi.org/10.3390/fl2060693>

- [19] Chen F, Han G, Li Q, Gao X, Cheng W (2017) High-temperature hot air/silane coupling modification of wood fiber and its effect on properties of wood fiber/HDPE composites. *Materials* 10(3):1–17. <https://doi.org/10.3390/ma10030286>
- [20] Chen F, Li Q, Gao X, Han G, Cheng W (2017) Impulse-cyclone drying treatment of poplar wood fibers and its effect on composite material's properties. *BioResources* 12(2):3948–3964
- [21] Jamaluddin N, Hsu YI, Asoh TA, Uyama H (2021) Effects of acid-anhydride-modified cellulose nanofiber on poly(lactic acid) composite films. *Nanomaterials* 11(3):1–15. <https://doi.org/10.3390/nano11030753>
- [22] Stamm AJ, Tarkow H (1947) Dimensional stabilization of wood. *J Phys Colloid Chem* 51(2):493–505. <https://doi.org/10.1021/j150452a016>
- [23] Matsuda H (1987) Preparation and utilization of esterified woods bearing carboxyl groups. *Wood Sci Technol* 21(1):75–88. <https://doi.org/10.1007/BF00349719>
- [24] Kim I, Thybring EE, Karlsson O, Jones D, Mantanis GI, Sandberg D (2021) Characterisation of moisture in scots pine (*Pinus sylvestris* L.) sapwood modified with maleic anhydride and sodium hypophosphite. *Forests* 12(10):1–9. <https://doi.org/10.3390/f12101333>
- [25] Gallardo-Cervantes M, González-García Y, Pérez-Fonseca AA, González-López ME, Manríquez-González R, Rodrigue D, Robledo-Ortiz JR (2021) Biodegradability and improved mechanical performance of polyhydroxyalkanoates/agave fiber biocomposites compatibilized by different strategies. *J Appl Polym Sci* 138(15):1–14. <https://doi.org/10.1002/app.50182>
- [26] Jebrane M, Sèbe G (2008) A new process for the esterification of wood by reaction with vinyl esters. *Carbohydr Polym* 72(4):657–663. <https://doi.org/10.1016/j.carbpol.2007.10.001>
- [27] Lee SH, Ohkita T, Kitagawa K (2004) Eco-composite from poly (lactic acid) and bamboo fiber. *Holzforschung* 58(5):529–536. <https://doi.org/10.1515/HF.2004.080>
- [28] Guo Y, Chen JQ, Su M, Hong JG (2018) Bio-based plastics with highly efficient esterification of lignocellulosic biomass in 1-methylimidazole under mild conditions. *J Wood Chem Technol* 38(4):338–349. <https://doi.org/10.1080/02773813.2018.1488876>
- [29] Fambri L, Pegoretti A, Fenner R, Incardona SD, Migliaresi C (1997) Biodegradable fibres of poly(l-lactic acid) produced by melt spinning. *Polymer* 38(1):79–85. [https://doi.org/10.1016/S0032-3861\(96\)00486-7](https://doi.org/10.1016/S0032-3861(96)00486-7)

Publisher's Note Springer Nature remains neutral with regard to jurisdictional claims in published maps and institutional affiliations.